Tunneling-induced Ground Subsidence Revealed by Spaceborne and UAV-borne Synthetic Aperture Radar Interferometry: A Case Study in Shenzhen, China

Mingshan Mo¹, Bochen Zhang¹, Linjie Zhang¹, Shuai Yuan¹, Songbo Wu², Gan Qin³

Keywords: UAV-SAR, PS-InSAR, Tunneling, deformation, Shenzhen.

Abstract

During the construction of subway lines, the excavation process of tunneling can sometimes cause safety hazards such as ground subsidence and cracks in surrounding buildings and roads along the excavation line. Therefore, monitoring the ground deformation along the tunneling lines is crucial to ensuring the safety of the surrounding infrastructures. Driven by the rapid advancement of unmanned aerial vehicle (UAV) technology, UAVs as remote sensing platforms equipped with miniature synthetic aperture radar have become an effective solution for studying ground subsidence associated with construction. Compared with traditional methods, UAV-based remote sensing platforms have significant advantages such as flexible deployment, high resolution, and short revisit time. This study used a UAV as the remote sensing platform with a miniSAR for data acquisition and applied the differential synthetic aperture radar interferometry (DInSAR) method to monitor surface deformation in the area along Longcheng avenue, Longgang district, Shenzhen, China. Results show that deformation in the anomalous area ranges from -2.67 cm to 1.05 cm. Finally, cross-validation was performed using results from persistent scatterers interferometry (PSI). Deformation analysis results for part of the tunneling route on Longcheng Avenue in Longgang District, Shenzhen, China, demonstrated that the UAV-SAR method can effectively monitor deformation associated with underground constructions, i.e., tunneling and grouting.

1. Introduction

Ground subsidence from construction activities is crucial for urban infrastructure safety and early warning of constructioninduced geological hazards. Remote sensing techniques have proven effective in monitoring such subsidence with high spatiotemporal resolution. Synthetic aperture interferometry (InSAR) has become one of the core tools for large-scale ground deformation monitoring, leveraging its allweather and all-day observation capabilities (Zhang et al., 2021; Wu et al., 2023). Spaceborne SAR systems exhibit unique advantages in long-term ground deformation monitoring due to their stable orbital coverage and global observation capacity, with applications in monitoring the stability of infrastructures and damage from geohazards (Osmanoğlu et al., 2016; Xiong et al., 2021; Zhang et al., 2025). In tunnel construction, the effectiveness of InSAR is validated by integrating advanced algorithms. Barla et al., combined persistent scatterers interferometry (PSI) and SqueeSAR to monitor ground movements, providing a robust framework for real-time deformation analysis (Barla et al., 2016). In the Northern Apennines, Italy, Bayer et al., applied StaMPS and SBAS techniques to link landslide reactivation with tunnel advancement. This demonstrates how InSAR can reveal spatio-temporal correlations between construction activities and geological hazards (Bayer et al., 2017). In urban contexts, such as London's Crossrail project, Giardina et al., used MT-InSAR to assess settlement damage, emphasizing its utility in soil-structure interaction analysis (Giardina et al., 2017). Liu et al., combined PSI with machine learning to analyze twin-tunnel excavation in Los Angeles, uncovering the critical role of overlying artificial fill thickness in uneven subsidence (Liu et al., 2022).

However, due to the limitation of the revisit cycles, spaceborne platforms face challenges in high-frequency dynamic

deformation scenarios, which make it unsuitable for studying the dynamic deformation induced by the underground construction.

In contrast to spaceborne systems, SAR systems mounted on unmanned aerial vehicles (UAVs) can provide an innovative solution for local high-precision deformation monitoring through flexible platforms and high-resolution imaging (Essen et al., 2012). It can obtain radar images with sufficient temporal resolution (Ding et al., 2020), i.e., minutes level to several minutes and significantly reduce the cost of acquiring high-resolution satellite imagery. UAV-SAR can precisely monitor ground subsidence with fine flight conditions (Xie et al., 2024). Therefore, it is an ideal technique for measuring ground subsidence in urban areas, especially regions under construction, such as tunneling.

However, monitoring ground deformation with UAV-SAR still has many challenges, i.e., non-linear trajectory of UAVs, high precision of image coregistration, and baseline-related phase contributions, especially in urban scenarios. In this study, the ground deformation of the tunneling section of Longcheng avenue in Shenzhen metro line 16 is revealed by both spaceborne and UAV-borne InSAR. The feasibility of using the UAV-SAR method for monitoring subsidence of urban metro lines was evaluated. Moreover, ground deformation obtained by applying PSI to spaceborne SAR images are used for cross-validation.

2. Research Area and Instrument

As a typical representative of rapid urbanization in China, Shenzhen has a massive scale of metro network construction, and ground subsidence induced by shield tunneling has become a significant threat to urban safety (Zhao et al., 2023). It is necessary to monitor the ground deformation along the subway lines, which is an essential measure to ensure the safe operation

¹ College of Civil and Transportation Engineering, Shenzhen University, 518060 Shenzhen, China, 1360501357@qq.com; bochen.zh@gmail.com; linjiezh.25@gmail.com; 2367772886@qq.com

² Department of Land Surveying and Geo-Informatics, The Hong Kong Polytechnic University, Kowloon, Hong Kong, China, lssongbo.wu@polyu.edu.hk

³ Shenzhen Technology Institute of Urban Public Safety, Shenzhen 518023, China, gqin@whu.edu.cn

of the subway and protect the surrounding infrastructure (Wang et al., 2022; Zhang et al., 2023). In this study, we select a tunneling route on Longcheng avenue in Longgang district, Shenzhen, China, as the study area, as shown in Figure 1. In this area, we found some fissures around the roads and on the surrounding buildings.

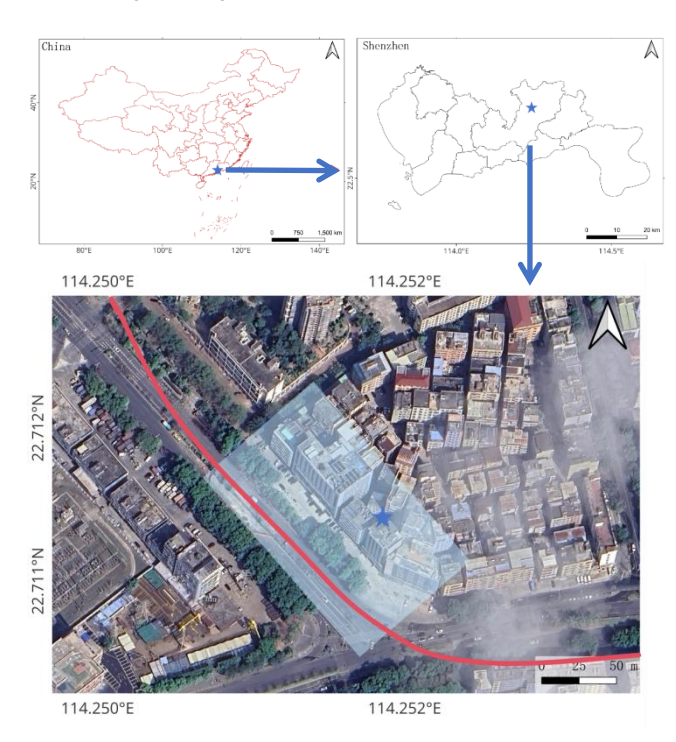


Figure 1. The location of the study area. The red curve represents the route of the shield machine. The blue stars denote locations of building settlements and wall peeling.



Figure 2. Experimental equipment.

The experimental equipment used in this study is shown in Figure 2. The miniature SAR experiment used X-band (wavelength of 3.11 cm) UAV-SAR, named SZU-X, with an imaging resolution of 0.15 m. Detailed parameters are presented in Table 1. During our experiment, a hexacopter drone was deployed over Longcheng Avenue in Longgang District, Shenzhen, located above the tunneling route of Shenzhen Metro Line 16, to monitor

the deformation of the surrounding buildings along the underconstruction subway lines.

Parameter	Content (Unit)	
Center Frequency	X-band (9.6 GHz)	
Bandwidth	1.2 GHz	
Radar System	FMCW	
Polarization Mode	HH, HV , VH , VV	
Imaging Resolution	$0.15 \text{ m} \times 0.15 \text{ m}$	
Maximum Detection	6 km	
Distance		
Maximum Swath Width	3 km	
Power Consumption	≤120 W	
Weight	\leq 4.0 kg	
Operating Temperature	-20°C - +50°C	

Table 1. Equipment parameters

3. Method

In the experiment, the monitoring area and flight route were planned according to the direction of the tunneling line and geological conditions to ensure comprehensive and pertinent data collection (Nex et al., 2014). The drone flew along the planned route, and UAV-SAR collected the data. Differential InSAR (DInSAR) techniques extracted ground deformation maps. The specific data processing flow is shown in Figure 3. GNSS and IMU data acquired by UAV-SAR were imported into professional data processing software for geodetic adjustment to improve orbital accuracy. The single-look complex (SLC) SAR images were focused using the post-processing position and posture information. After generating SLC data, traditional crosscorrelation algorithms were employed to coregister master and slave images. However, due to the non-linear trajectory of the drone, it is challenging to coregister well for the whole frame of SLCs. We only cut the small data area near the region of interest to realize the coregistration. Subsequently, interferometric coherence was estimated, and adaptive filtering was applied to enhance the quality of the interferogram. Phase unwrapping was achieved via the minimum cost flow (MCF) algorithm combined with a coherence mask. Finally, unwrapped phases were converted to line-of-sight (LOS) deformations, fully extracting ground deformation information from UAV-SAR imagery.

To compare the results from UAV-SAR, multitemporal InSAR data from spaceborne SAR data, Sentinel-1 from January 2024 to March 2025, were also processed. We use the Stanford method for persistent scatterers (StaMPS) software package to perform the PSI method (Hooper et al., 2007). A workflow description and parameter specifications are provided, with the processing flowchart shown in Figure 4. In the PSI processing, PS points were identified using the amplitude dispersion index with a threshold of 0.4. Following the phase noise estimation to derive temporal coherence for candidate points, the percentage of random phase pixels was used to filter candidates further. Given the urban nature of the study area, a maximum acceptable percentage of 50% was set for pixels with random phase.

Subsequently, PS points that exhibited phase stability only in certain interferograms and pixels displaying PS-like

characteristics due to adjacent PS point influence were removed. DEM error-induced phase correction was performed after determining the final set of PS points using the aforementioned method, followed by phase unwrapping. Finally, the phase noise induced by atmospheric delays was removed through spatiotemporal low-pass filtering for atmospheric correction.

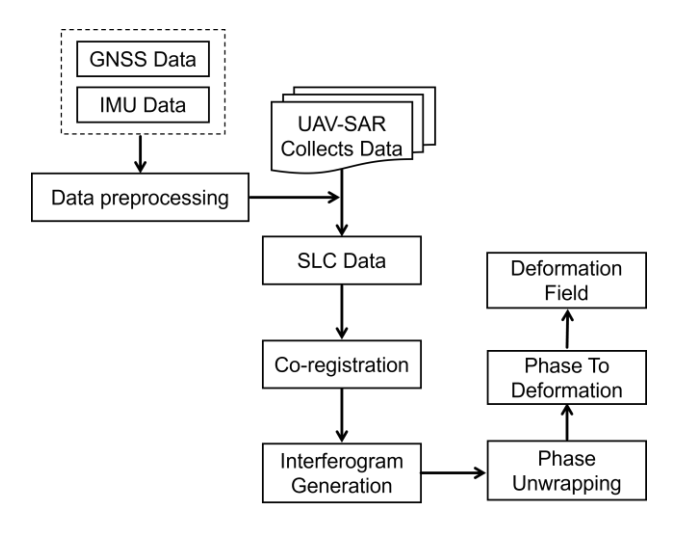


Figure 3. UAV-InSAR processing flow.

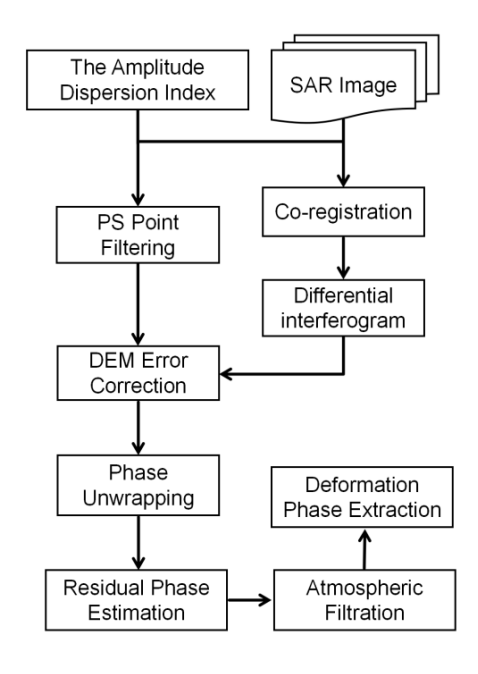


Figure 4. PSInSAR processing flow.

4. Results and Analysis of UAV-InSAR

Data acquisition was completed on December 14, 2024. During the experiment, the UAV flew at a speed of 10 m/s and an altitude of 150 m above the ground, with the SAR image swath width approximately 400 meters.

Following geodetic adjustment, new flight tracks were generated based on the input GNSS and IMU data, exhibiting a slight downward shift relative to the original track. Since the position of the drone was determined by GNSS mode, the adjustment accuracy was relatively low, approximately 44.59%. The

adjustment results are shown in Table 2. Using the RTK mode in other scenarios increases the adjustment accuracy up to 99%.

As expected, the UAV-SAR acquires three high-resolution images with fine details covering the ROI. Within the ROI, we selected a local area of the Blueprint Garden Hotel in Longgang District to test the feasibility of InSAR in obtaining the deformation results. Figure 5(a) and (b) show the interferogram pairs' mean coherence and average intensity, respectively. Figure 5(c) shows the interferograms of the three pairs, namely 20241214T180846-20241214T181240, 20241214T180846-20241214T181437, and 20241214T181240-20241214T181437. In the InSAR interferograms, abnormal signals can be observed as highlighted by the red and black boxes in Figure 5(c). These abnormal signals correspond to deformation of the same area, which is calculated to range from -2.67 cm to 1.05 cm by using interferometric 20241214T181240pair of 20241214T181437. The deformation signal is suspected to be caused by tunneling operations and grouting in this area.

It should be noted that several error sources in the UAV-InSAR results should be addressed in future investigations. For instance, inconsistencies in orbit alignment during UAV missions give rise to registration discrepancies and baseline errors, which constitute the primary error sources in this study.

Significant building subsidence and wall plaster detachment were observed during the field investigation in the experimental area, as shown in Figures 6(a) and (b). This observation is consistent with the deformation trends derived from UAV-SAR data. Thirtyone days after the completion of experimental data acquisition, a collapse occurred on the road surface within the study area. The collapsed region reported approximately 3 meters in length, 2 meters in width, and 1 meter in depth, as depicted in Figure 6(c). In the satellite imagery of Figure 6, the pentagram marks the area with building displacement and wall plaster detachment, while the red rectangle denotes the road collapse region. These findings validate the effectiveness of our monitoring methodology and the necessity of monitoring the shield machine route.

Statistics	Min	Max	Mean
Baseline length	0.02	0.61	N/A
Number of GPS	4	7	5
Number of GLONAS	S 0	4	3
Number of QZSS	0	0	0
Number of BDS	0	7	3
Number of Galileo	0	0	0
PDOP	1.79	4.78	2.81
QC Solution	10.00	10.00	N/A
Fixed Epoch: 659s	Float Epoch: 809s	. No	Solution: 10s
Fixed Solution:	Float Solution:	tion: No Solution:	
44.59%	54.74%		0.68%

Table 2. The adjustment of the positions of the drone.

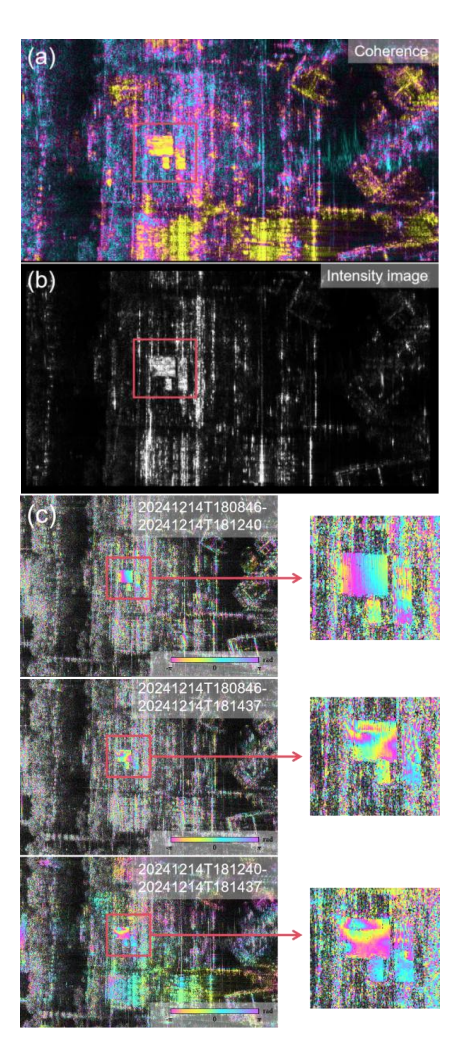


Figure 5. Experimental results of interferometric measurements.

(a) Mean coherence, (b) Average intensity, (c) Interferograms formed using the three UAV-SAR images.

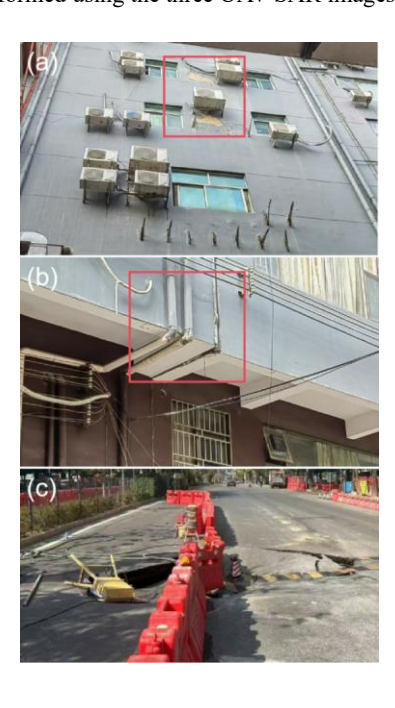


Figure 6. The field investigation. (a) Wall plaster detachment, (b) building displacement, (c) road collapse.

5. Results from Spaceborne InSAR

This study employs spaceborne InSAR to validate the reliability and precision of UAV-InSAR measurements. This is achieved by applying PSInSAR processing to 28 Sentinel-1A SAR images acquired from January 2024 to March 2025. The image acquired on August 14, 2024, was selected as the primary image, while the remaining 27 images served as secondary images for interferometric processing. The primary error source of this method is atmospheric delay error, which has been effectively mitigated through atmospheric correction. Figure 7 presents the deformation rates, with the red box denoting the Blueprint Hotel Garden. Figure 7 shows that the deformation rate of the Blueprint Hotel Garden ranges from -6.9 mm/year to -2.1 mm/year. Two points (P1, P2) with the most severe pavement subsidence and one point (P3) with the most significant roof deformation of the hotel were selected for time-series analysis, and the results are shown in Figure 8. The time-series results indicate that all three points exhibit a subsidence trend, with cumulative deformations ranging from 5 to 9 mm, while seasonal variations are also observed.

These results differ from the UAV-InSAR results, where the deformation rates exhibit larger deviations. The following two factors can primarily cause this discrepancy: a) The observation frequency of UAV-SAR typically refers to the time interval for the UAV to complete a flight path (e.g., once every 5 minutes), whereas the revisit period of Sentinel-1 is 12 days, leading to a significant disparity in temporal resolution. Thus, deformation signals monitored by UAV-SAR may represent transient deformations. For example, subsidence induced by tunneling may rebound after grouting. Spaceborne InSAR cannot capture this transient deformation. B) There are still some challenges for processing UAV-SAR data with fine precision, especially in urban scenarios with high-rise buildings. The derived deformation results may be undermined by inaccurate coregistration resulting from nonlinear UAV flight trajectories or orbital baseline errors.

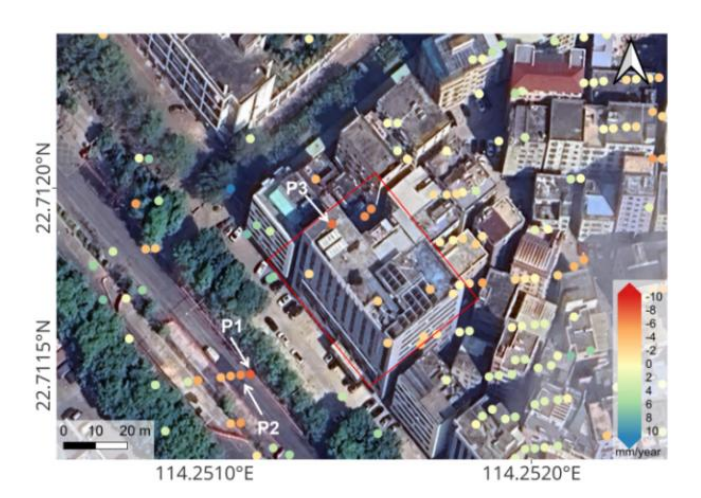


Figure 7. The red box denoting the Blueprint Hotel Garden shows the deformation rate results.

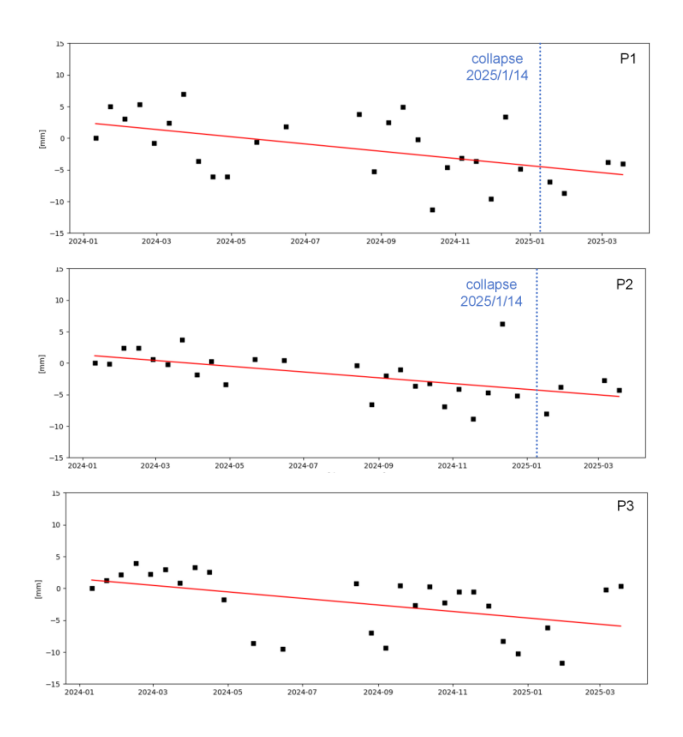


Figure 8. Time-series results at P1, P2, and P3.

6. Conclusion

Ground deformation is often associated with underground constructions, i.e., tunnelling and grouting. Monitoring the ground deformation is essential for ensuring the safety of its operation and the surrounding infrastructures. In this study, we demonstrated that UAV-SAR can be a suitable tool for monitoring the ground deformation in a tunneling scenario. The tunneling-induced deformation in the Longgang district of Shenzhen, China, was revealed by spaceborne and UAV-borne InSAR. Compared with spaceborne InSAR and ground-based SAR technologies, UAV-SAR features a more flexible working mode, serving as a highly beneficial technical supplement for deformation measurement. It can provide high-quality images while mitigating the long revisit period constraint of spaceborne InSAR. Nevertheless, the technology still has inherent limitations, including high-precision positioning and attitude determination, UAV motion induced by unstable airflow, image coregistration errors due to nonlinear movement, baseline and elevation errors from orbital misalignment, and atmospheric delay errors caused by fluctuating atmospheric conditions. Future UAV-SAR deformation monitoring research will address these limitations to overcome technical bottlenecks and gradually achieve highprecision ground deformation monitoring.

Acknowledgements

This work was supported by the National Natural Science Foundation of China (Grant 42304014), the Guangdong Basic and Applied Basic Research Foundation (No. 2025A1515012040), and the University Grants Council of the Hong Kong Polytechnic University (1-BD2S).

References

Barla, G., Tamburini, A., Del Conte, S., Giannico, C., 2016: InSAR monitoring of tunnel induced ground movements. *Geomechanics and Tunnelling*. 9, 15–22.

Bayer, B., Simoni, A., Schmidt, D., Bertello, L., 2017: Using advanced InSAR techniques to monitor landslide deformations induced by tunneling in the Northern Apennines, Italy. *Engineering Geology.* 226, 20–32.

Ding, L., Ding, C., Tang, L., Wang, X., Qu, J., Wu, R., 2020: A W-Band 3-D Integrated Mini-SAR System With High Imaging Resolution on UAV Platform. *IEEE Access.* vol. 8, 113601–113609.

Essen, H., Johannes, W., Stanko, S., Sommer, R., Wahlen, A., Wilcke, J., 2012: High resolution W-band UAV SAR. 2012 IEEE International Geoscience and Remote Sensing Symposium. 5033–5036.

Giardina, G., Milillo, P., DeJong, M., Perissin, D., Milillo, G., 2019: Evaluation of InSAR monitoring data for post-tunnelling settlement damage assessment. *Struct Control Health Monit.* 26.

Hooper, A., Segall, P., Zebker, H., 2007: Persistent scatterer interferometric synthetic aperture radar for crustal deformation analysis, with application to Volcán Alcedo, Galápagos. *Journal of Geophysical Research: Solid Earth.* 112(B7).

Liu, L., Zhou, W., Gutierrez, M., 2022: Mapping Tunneling-Induced Uneven Ground Subsidence Using Sentinel-1 SAR Interferometry: A Twin-Tunnel Case Study of Downtown Los Angeles, USA. *Remote Sensing*. 15, 202.

Nex, F., Remondino, F., 2014: UAV for 3D mapping applications: a review. *Appl Geomat.* 6, 1–15 (2014).

Osmanoğlu, B., Sunar, F., Wdowinski, S., Cabral-Cano, E., 2016: Time series analysis of InSAR data: Methods and trends. *Isprs journal of photogrammetry and remote sensing*. 115, 90-102.

Wang, R., Yang, M., Dong, J., Liao, M., 2022: Investigating deformation along metro lines in coastal cities considering different structures with InSAR and SBM analyses. *International Journal of Applied Earth Observation and Geoinformation*. 115, 103099.

Wu, S., Zhang, B., Ding, X., Zhang, L., Zhang, Z., Zhang, Z., 2023: Radar interferometry for urban infrastructure stability monitoring: from techniques to applications. *Sustainability*. 15(19), 14654.

Xiong, S., Wang, C., Qin, X., Zhang, B., Li, Q., 2021: Timeseries analysis on persistent scatter-interferometric synthetic aperture radar (PS-InSAR) derived displacements of the Hong Kong–Zhuhai–Macao Bridge (HZMB) from Sentinel-1A observations. *Remote Sensing*. 13(4), 546.

Xie, X., Deng, Y., Tian, W., 2024: Preliminary Result of Multiplane Interferometry Topography Measurement with UAV InSAR. *IEEE International Conference on Signal, Information and Data Processing (ICSIDP)*. 1–5.

Zhang, B., Ding, X., Amelung, F., Wang, C., Xu, W., Zhu, W., Baba, T., 2021: Impact of ionosphere on InSAR observation and coseismic slip inversion: Improved slip model for the 2010 Maule. Chile, earthquake. *Remote Sensing of Environment.* 267, 112733.

Zhang, B., Liao, X., Zhang, J., Xiong, S., Wang, C., 2023: Megalopolitan-scale ground deformation along metro lines in the

Guangdong-Hong Kong-Macao Greater Bay Area, China, revealed by MT-InSAR. *International Journal of Applied Earth Observation and Geoinformation*. 122, 103432.

Zhao, Y., Chen, X., Hu, B., Huang, L., Fan, J., 2023: Evolution of tunnel uplift and deformation induced by an upper and collinear excavation: A case study from Shenzhen metro. *Transportation Geotechnics*. 39 100953.

Zhang, J., Liu, Y., Zhang, B., Xiong, S., Wang, C., Wu, S., Zhu, W., 2025: Spatiotemporal-grained quantitative assessment of construction-induced deformation along the MTR in Hong Kong using MT-InSAR and iterative STL-based subsidence ratio analysis. *International Journal of Applied Earth Observation and Geoinformation*. 136, 104342.